Heliyon 6 (2020) e04730

Contents lists available at ScienceDirect

Heliyon

journal homepage: www.cell.com/heliyon

Research article

# Proficient dye removal from water using biogenic silver nanoparticles prepared through solid-state synthetic route

Mohsen Rahimi Sharbaf Moghadas [a], Elaheh Motamedi [b,*], Jaber Nasiri [a], Mohammad Reza Naghavi [a,**], Manije Sabokdast [a]

[a] Department of Agronomy and Plant Breeding, Agricultural and Natural Resources College, University of Tehran, Karaj, Iran
[b] Department of Nanotechnology, Agricultural Biotechnology Research Institute of Iran (ABRII), Agricultural Research, Education and Extension Organization (AREEO), Karaj, Iran

ARTICLE INFO

*Keywords:*
Nanotechnology
Natural product chemistry
Organic chemistry
Environmental chemistry
Wastewater management
Silver nanoparticles
Green synthesis
*Mentha* piperita
Nanoadsorbent
Crystal violet
Water treatments

ABSTRACT

An environmentally benign, one-pot and highly scalable method was presented to produce biogenic silver nanoparticles (Ag NPs) using the solid-state synthetic route. Four plant-derived candidate bio-reductants (*i.e., Datura stramonium, Papaver orientale, Mentha piperita,* and *Cannabis sativa*) were investigated to compare the efficiency of solid-state route and typical solution method. *M. piperita* was selected as the best plant resource to produce totally pure and uniform Ag NPs (average diameter of 15 nm) without any aggregation. The purity and size of biogenic Ag NPs, were tailored by adjusting the *M. piperita* leaf powder/silver nitrate weight ratio and temperature. The as-synthesized Ag NPs were effectively utilized as an eco-friendly nanoadsorbent in water remediation to remove a model dye (i.e., crystal violet). The key factors affecting on the sorption process (i.e., nanoadsorbent dosage, temperature, pH, dye initial concentration, and shaking time) were investigated. The pseudo-second-order kinetic model was well fitted to the sorption process and at the optimum sorption conditions, based on the Langmuir model, the adsorption capacity was found to be 704.7 mg/g. The current, cost effective and feasible method could be considered as an applicable strategy to produce green, reusable and proficient Ag NPs as nanoadsorbents for removal of dyes from contaminated water.

## 1. Introduction

Recently, silver nanoparticles (Ag NPs) have attracted extensive research and industrial interests, mainly due to their vast beneficial applications including surface-enhanced Raman scattering substrates (SERS), optical sensors, catalysts, and biomarkers [1, 2]. Besides, strong antimicrobial activity of Ag NPs causes a growing list of their consumer products like cosmetics, textiles, sterilizers and testing tools, food packaging, medical implants, pest and disease management in plants, and so on [3, 4, 5]. In this regards, the development of green and eco-friendly synthetic processes of Ag NPs could reduce the environmental risks and potential adverse effects of chemical-based methods on the environment [6, 7, 8, 9, 10]. In fact, upon the first report about using plant extracts (*Medicago sativa*) in the synthesis of metallic nanoparticles, much more interests have been attracted to this subject, as abundant plant species have been extensively employed for the fabrication of green synthesized of nanoparticles [10]. Particularly, the application of herbal plants as the valuable resources of secondary metabolites with bio-medicinal activity and minimal toxicity have been proven in producing of biogenic Ag NPs [11]. Besides, plant-mediated synthesis can be used for mass production of pure Ag NPs with narrow size distribution and well-defined morphology without any contamination or toxic by-products [12]. More specifically, synthesis of Ag NPs via green and environmentally benign procedures is important for their utilization in medical, agrochemical, environmental and biotechnological fields [12, 13]. Plant extracts as renewable precursors has been recently considered as one of the best proecological preparation tools of Ag NPs, owing to their low-cost, simplicity, eco-friendly and readily scaled-up nature [14, 15, 16]. Biomolecules present in plant extracts (e.g., alkaloids, glycosides, terpenoids, flavonoids, coumarins, ubiquinones, tannins, etc.) and co-enzymes are responsible for the reduction of silver ions and turning them into Ag NPs through a one-pot green process [3, 13, 17, 18]. Nevertheless, most of these plant extract-based approaches have been conducted in liquid media in which the aqueous extracts are mixed with

* Corresponding author.
** Corresponding author.
*E-mail addresses:* motamedi.elaheh@gmail.com, motamedi@abrii.ac.ir (E. Motamedi), mnaghavi@ut.ac.ir (M.R. Naghavi).

https://doi.org/10.1016/j.heliyon.2020.e04730
Received 5 March 2020; Received in revised form 16 March 2020; Accepted 12 August 2020

the appropriate silver salt solution. Although such solution phase methods could effectively produce Ag NPs with uniform particle sizes, they usually suffer from some crucial drawbacks such as: 1) agglomeration of colloidal particles; 2) needing to add a protecting agent/surfactant; 3) requiring very low concentrations of the metal in the dispersion to achieve stable colloids; 4) demanding large amounts of solvent or dispersion media, particularly in the commercial manufacturing of Ag NPs; 5) unavoidable production of byproducts because of the presence of impurities/unwanted species during preparation of the plant extracts [19, 20, 21]. Alternatively, non-aqueous synthesis of Ag NPs through thermal decomposition [2, 20, 22, 23] or mechanochemical processes [24, 25, 26, 27] could overcome such difficulties through incubation of silver precursors with plant derived bio-reducers in a solid phase. The produced Ag NPs have been reported to be pure, uniform, and highly stable without any aggregation. Besides, the solid-state method could facilitate large scale production of biogenic Ag NPs by elimination of solvents from the preparation process and decreasing the production cost of the final nanoparticles [19, 20, 21, 28].

On the other hand, dyes have been proven as one of the main reasons of water pollution because of their widely industrial utilization. So, effective and economical dye removal from water have been turned into an important and interesting research topic [29]. Among several methods have been proposed for the remediation of dye-polluted waters, the adsorption-based technique has been suggested as one of the best practical approaches [30]. In this sense, the demand for application of metal nanoparticles, particularly Ag NPs, as nanoadsorbent have been raised owing to their unique properties [29, 31, 32].

In our earlier report, we compared and contrasted the efficiency of two green synthetic routes (i.e., solid vs. solution synthetic routes) for the preparation of Ag NPs using *Ferula persica* [28]. The interesting simultaneous effects of tissue types and reaction media on the biological synthesis of Ag NPs motivated us to follow our studies by focusing on assessing proficient and effective natural resources to produce biogenic Ag NPs as green and practical nano-adsorbent for water remediation. Hence, in the current study, the proficiency of four plant resources (*i.e. Datura stramonium* L., *Papaver orientale.* L., *Mentha piperita* L., and *Cannabis sativa* L.) was explored in the synthesis of biogenic Ag NPs using the solid-state method. Although there are some reports on the Ag NPs green synthesis by these four medicinal plants through solution phase method [33, 34, 35], the production of Ag NPs via solid-state synthetic route using such plant materials has not been reported yet. Our finding demonstrated that *Mentha piperita* L. was the best plant resource of choice to manufacture pure Ag NPs with uniform size and no aggregation using the solid-state method. Furthermore, the efficiency of as-prepared biogenic Ag NPs was evaluated in the removal of crystal violet (CV) as a model dye, from water. The superior performance of Ag NPs, in CV removal, could result in a high throughput and low-cost approach to produce biogenic Ag NPs with potential applications in water remediation.

## 2. Materials and methods

### 2.1. Plant materials and chemicals

*Datura stramonium* L., *Papaver orientale.* L., *Mentha piperita* L., *Cannabis sativa* L. samples were collected from the research field of the University of Tehran, Karaj, Iran (Sep, 2016). At first, plant samples were rinsed with water, the leaves were air-dried, and then grinded reaching to a

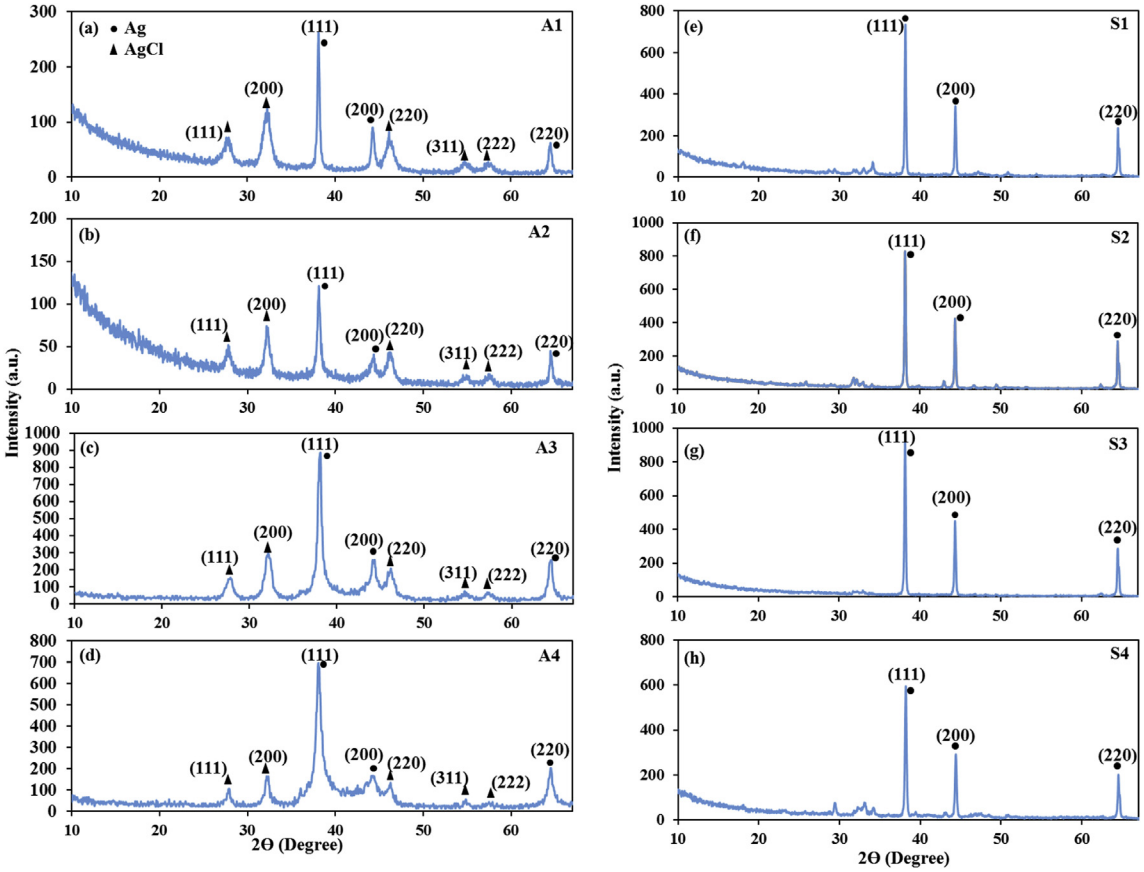


**Figure 1.** XRD patterns of Ag NPs synthesized using *D. stramonium, P. orientale., M. piperita,* and *C. sativa* through solution-phase method (a–d) and solid-satet route (e–h).

powdery solid. Silver nitrate ($AgNO_3$, Sigma–Aldrich) along with the other chemicals were of analytical grade.

### 2.2. Characterization of nanoparticles

To characterize the current green-synthesized Ag NPs, several characterization techniques were employed, as detailed below:

#### 2.2.1. Fourier-transform infrared (FTIR) spectroscopy

The functional groups of as-synthesized Ag NPs were characterized using FTIR spectroscopy (WQF-510 FTIR Spectrometer in the range of 400–4000 $cm^{-1}$).

#### 2.2.2. X-ray diffraction (XRD)

To monitor particle size of the current green-synthesized Ag NPs, XRD (Philips model: PW1730, $\lambda = 1.54056$ Å (Cu Ka irradiation), $2\Theta =$ 10–80°, step size of 0.02° $2\Theta$, 1 s scan step time) was employed. Moreover, the crystallite sizes (D) of samples were calculated from the line width of the (111) XRD peak by Scherrer's equation:

$$D = K\,\lambda / (\beta \times \cos\theta)$$

where, K is the shape factor, $\lambda$ is the wavelength of the x-ray, $\beta$ is the broadening of the diffraction line measured as half of its maximum intensity in radians and $\theta$ is the Bragg's diffraction angle.

#### 2.2.3. Field emission scanning electron microscopy (FESEM)

In order to evaluate the surface topology and elemental analysis of the current green-synthesized Ag NPs, a TESCAN MIRA II, FESEM with the 20 kV voltage was employed, which was equipped with EDX, energy dispersive X-ray, instrument (INCA, Oxford). Measuring the particle size distributions, the size of about 100 particles in the electron microscope images of each sample was estimated and correspond histograms were depicted.

#### 2.2.4. Ion Chromatography analysis

The concentrations of chlorine ion in the samples were analyzed by Ion Chromatography analysis (Metrohm Instrument).

#### 2.2.5. Transmission electron microscopy (TEM)

To acquire morphological/topological information regarding the current green-synthesized Ag NPs, the TEM images were provided by an EM208S Philips microscope with accelerating voltage of 100 kV.

### 2.3. Synthesis of biogenic Ag NPs using aqueous method

Firstly, for the preparation of each plant extract, 1.0 g of the leaf powder was added into a flask filled with the distilled water (30 mL), then the mixture temperature was raised to100 °C. After 15 min, the extract was filtered and then added to as-prepared 0.02 M solution of $AgNO_3$. The flask was wrapped in an aluminum foil to ensure darkness condition and then incubated (37 °C, 180 rpm, overnight). Afterwards, the resulting precipitates were collected via centrifugation (15 min, 6000 rpm), the resultant pellet was initially washed with absolute ethanol along with distilled water thrice and dried lastly at 80 °C for 10 h, in an oven. Finally, four Ag NPs samples were prepared from different plant extracts of *D. stramonium, P. orientale.* L., *M. piperita, C. sativa* which were nominated as A1, A2, A3, and A4, respectively.

### 2.4. Solid-state synthesis of Ag NPs

$AgNO_3$ salt (1.5 g) was weighed and mixed with the leaf powders of each plant separately, and the mixtures were thoroughly grinded using a mortar and pestle. The resultant mixture was heated for 3 h at 600 °C, in a furnace. After that, the samples were cooled down to ambient temperature and the collected precipitates were washed with ethanol and distilled water, and then oven dried (80 °C, 10 h). Similar to the aqueous method, four Ag NPs samples were prepared from different plant extracts of *D. stramonium, P. orientale, M. piperita, C. sativa* which were coded as S1, S2, S3, and S4, respectively.

### 2.5. Batch sorption experiments

For evaluation of the efficiency of synthesized Ag NPs in CV removal from water, different amounts of the best nanoadsorbent (i.e., 4, 6 and 8 mg) were added to CV solutions (2.0 mL, 1000 mg/L; pH ranged from 3.0 to 9.0). To study the sorption kinetic, the CV removal was measured at different contact times from 5 min to 2 h, in two different CV solutions with the initial concentrations of 500 and 750 mg/L. To analyze the sorption isotherms, CV solutions with different initial concentrations (500–1500 mg/L) were prepared, then Ag NPs were added to each solution and the mixtures were agitated for 2 h, at various temperatures (25, 34 and 45 °C). To adjust the initial pH of solutions, HCl (1.0 N) and NaOH (1.0 N) were utilized. The CV concentration after sorption experiments was calculated using UV-Vis spectrophotometer (Microplate reader, BioTek® Instruments Inc.) at $\lambda = 590$ nm. The values of $q_e$ (equilibrium CV sorption capacity; mg/g), and dye removal percentage (%) were estimated using the following equations of Eq. 1 and Eq. 2, respectively.

$$q_e = \frac{(C_0 - C_e)V}{M} \tag{1}$$

$$\text{Dye removal}(\%) = \frac{C_0 - C_e}{C_0} \times 100 \tag{2}$$

where $C_0$ (initial CV concentration, mg/L), $C_e$ (equilibrium CV concentration, mg/L), $V$ (volume of the solution, L) and $M$ (adsorbent weight, g) were employed, respectively.

To fit the kinetic and equilibrium data the nonlinear methods were used and $R^2$ (determination coefficient), $R^2_{adj}$ (adjusted determination coefficient) and *SD* (standard deviation of residues) were determined via the following Eqs. (3), (4), and (5) [36, 37].

$$R^2 = \left( \frac{\sum^n \left(q_{i,exp} - \overline{q}_{exp}\right)^2 \sum^n \left(q_{i,exp} - \overline{q}_{i,model}\right)^2}{\sum^n \left(q_{i,exp} - \overline{q}_{exp}\right)^2} \right) \tag{3}$$

$$R^2_{adj} = l - \left(1 - R^2\right) \cdot \left( \frac{n-1}{n-p-1} \right) \tag{4}$$

$$SD = \sqrt{\left( \frac{1}{n-p} \right) \cdot \sum_i^n \left(q_{i,exp} - q_{i,model}\right)^2} \tag{5}$$

where $\overline{q}$ is the average of experimental $q$ values, $q_{i,\ exp}$ is individual experimental $q$ value; $q_{i,\ model}$ is individual theoretical $q$ value estimated by the model; $p$ is the number of parameters in the fitting model; and n is the number of experiments.

### 2.6. Reusability of nanoadsorbent

Ag NPs (2 g/L) were added to CV solutions with the initial concentration of 1000 mg/L, and the mixtures were agitated (90 min) at room temperature. Then, the nanoadsorbents were separated by centrifugation and thoroughly washed with excess deionized water and ethanol. Next, the recovered Ag NPs were oven dried (80 °C) and reused for the next batch experiment cycle, at the same conditions.

**Table 1.** Calculated crystalline size of Ag NPs synthesized using different synthetic methods and plant extracts from Scherrer equation.

| Biogenic Ag NPs samples | Peak position | FWHM | Crystalline size (nm) |
|---|---|---|---|
| A1 | 38.11 | 0.3796 | 23.7 |
| A2 | 38.12 | 0.4844 | 18.6 |
| A3 | 38.04 | 0.6598 | 13.6 |
| A4 | 38.09 | 0.5859 | 15.4 |
| S1 | 38.15 | 0.2144 | 42.2 |
| S2 | 38.16 | 0.2001 | 45.3 |
| S3 | 38.16 | 0.2303 | 39.4 |
| S4 | 38.20 | 0.2486 | 36.6 |

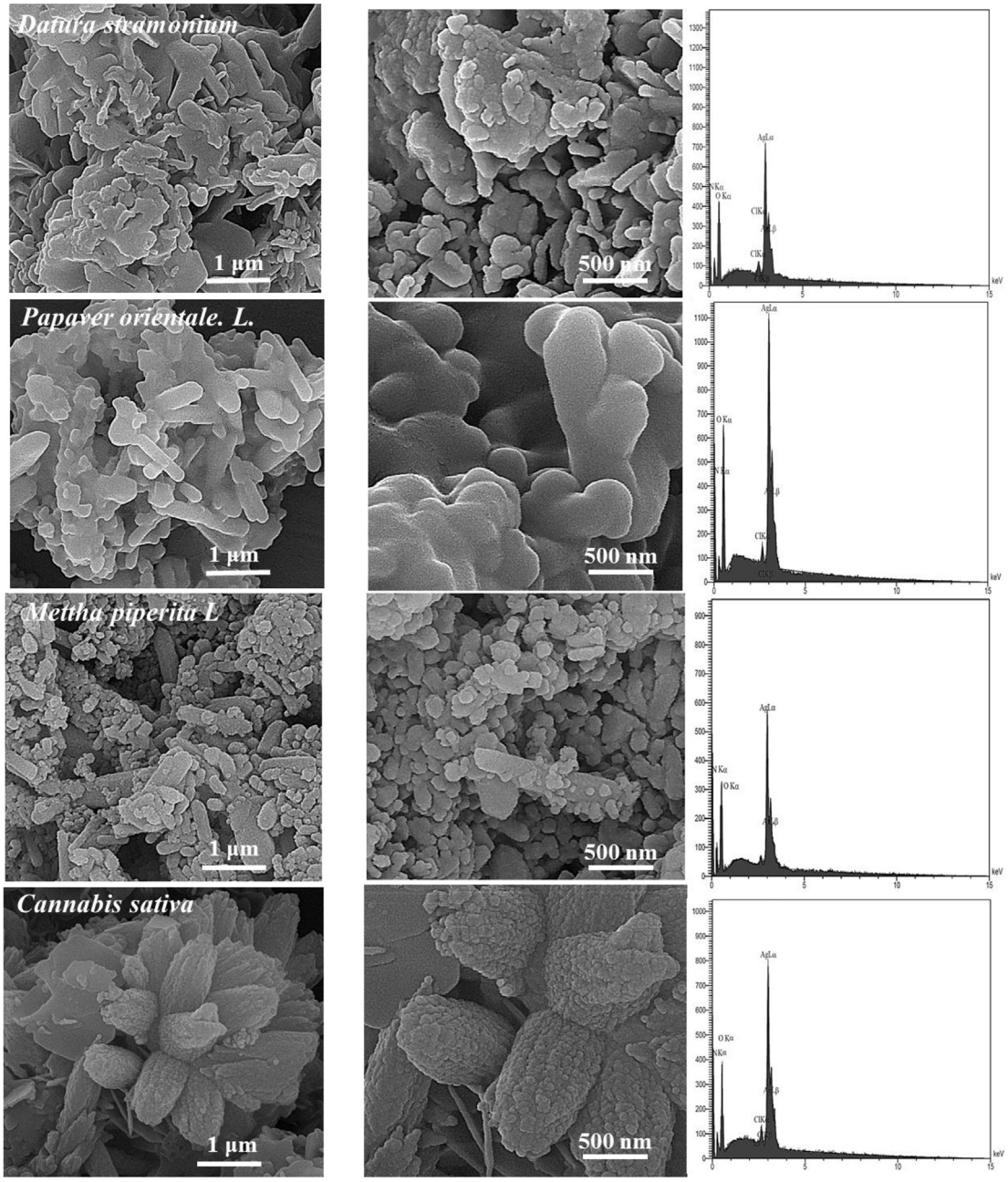


**Figure 2.** FESEM images of Ag NPs in two different magnifications synthesized using *D. stramonium, P. orientale, M. piperita,* and *C. sativa* (left) and their EDX spectrum (right).

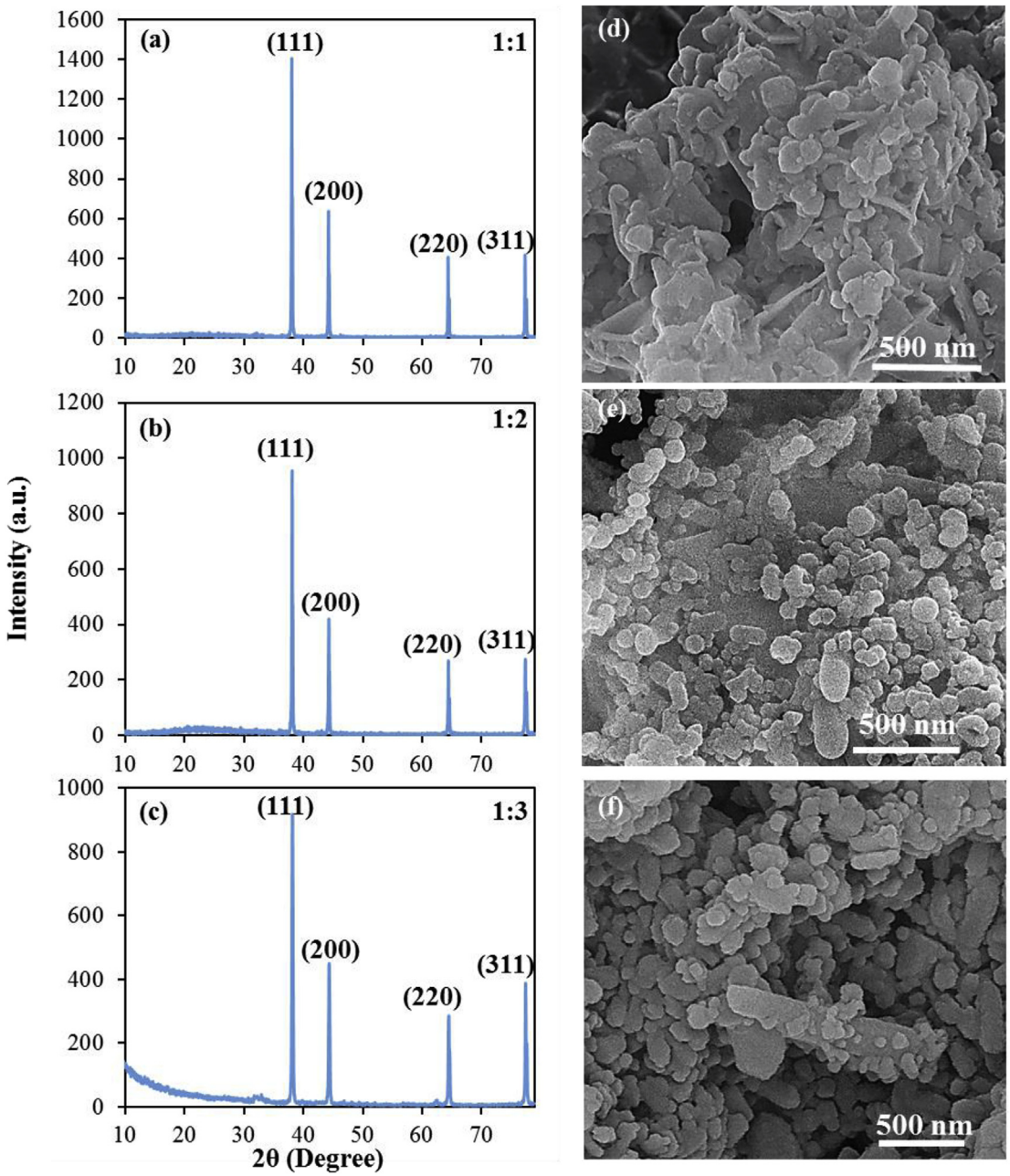


**Figure 3.** XRD patterns (a–c) and FESEM images (d–f) of solid-state synthesized Ag NPs by different feeding ratios of silver nitrate to *M. piperita* leaf ($m_{AgNO3}$: $m_{M.\ piperita\ powder}$ = 1:1, 1:2, and 1:3).

## 3. Results and discussion

### *3.1. Comparison between proficiency of solid-state and solution-phase method in production of biogenic Ag NPs*

XRD analyses clearly showed that the solid-state syntheses resulted in the Ag NPs with much less impurities and more crystallinity (Figure 1). XRD patterns of the nanoadsorbents synthesized via solid-state method (Figure 1e-h) displayed the prominent peaks at 38.10° (111), 44.38° (200), 64.54° (220), and 77.64° (311) which were indexed to Ag NPs. In contrast, in the XRD patterns of all the samples prepared through solution-phase route (Figure 1a-d), along with the Ag NPs signals, some intense diffraction peaks at 2θ = 28.11° (111), 32.04° (200), 46.06° (220), 55.22° (311), and 57.29° (222) were appeared which were indexed to AgCl. A small amount of AgCl could be detected also in the samples prepared by the solid-state approach (Figure 1e-h). These results could be attributed to the fact that within preparation of the aqueous plant extracts the chloride ions were involved. Similar results have been also reported in the previous works which employed these four plant extracts for the solution-phase synthesis of Ag NPs [33, 35, 38]. Furthermore, the average estimated crystallite size of each sample was calculated and presented in Table 1. The differences in XRD patterns of Ag NPs synthesized by different methods could be attributed to the fact that in the preparation of the leaf extracts for aqueous synthesis of Ag NPs, the presence of chloride ions in the extracts resulted in the synthesis of some AgCl impurities in the samples. However, in the solid-state route the biomaterials in dried leaf powders which caused the reduction of silver ions could be decomposed at elevated temperatures and their residuals separated from Ag NPs samples by washing process. Therefore, the XRD patterns of the samples produced by solid-state method showed just little peaks for impurities. Besides, the differences in the peak intensities in the XRD patterns of the samples synthesized via different

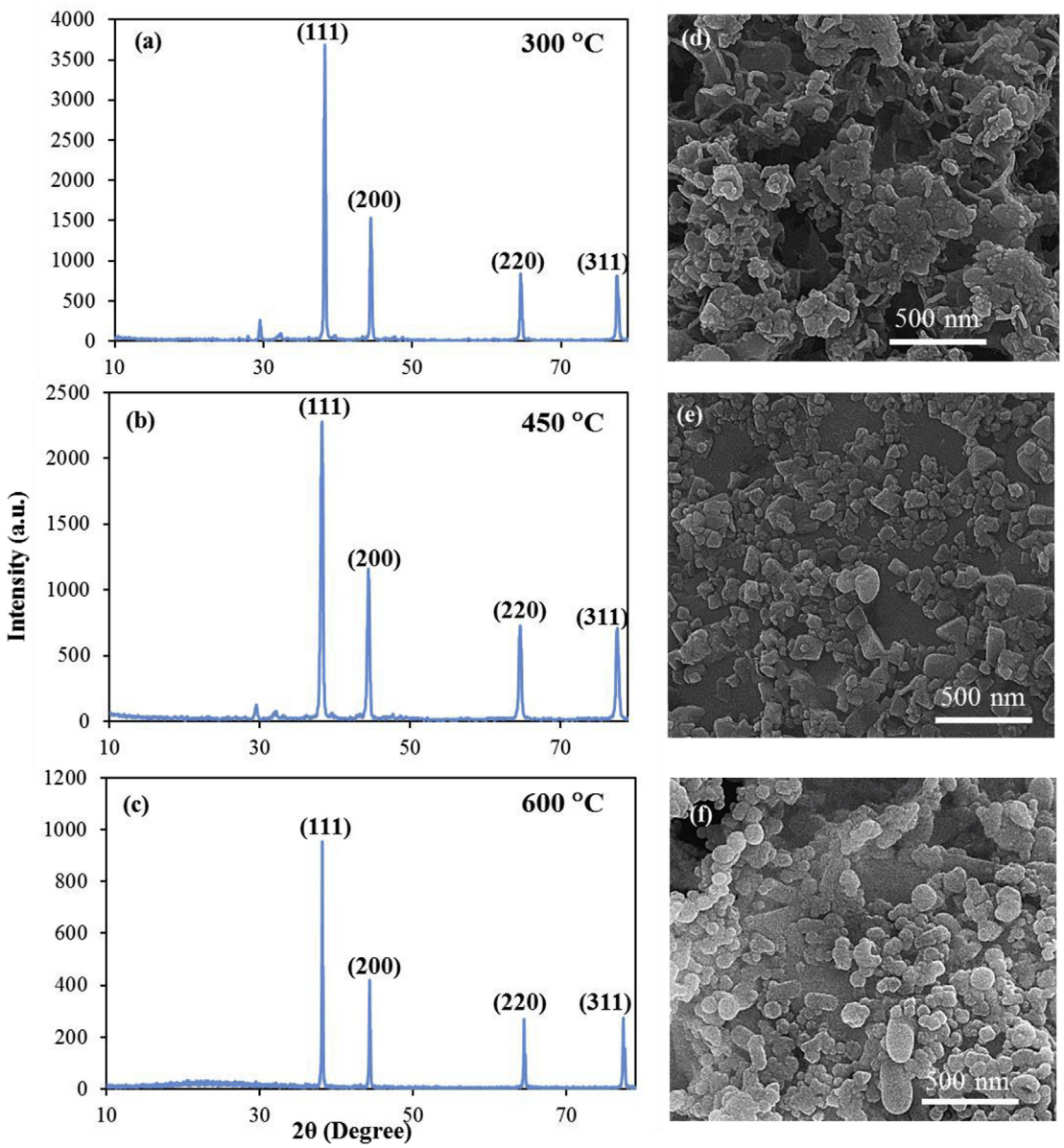


**Figure 4.** XRD patterns (a–c) and FESEM images (d–f) of solid-state synthesized Ag NPs by *M. piperita.* leaf powder ($m_{AgNO3}$: $m_{M.\ piperita\ powder}$ = 1:2), at different temperatures.

plant extracts in each method could be due to the biomaterials variability in each plant species studied here.

### 3.2. Selection of the best plant mediator for solid-state production of biogenic Ag NPs

In the next step, the morphological structure, size, and dispersity of Ag NPs prepared using solid-state route were analyzed via FESEM (Figure 2). The results showed that among four samples prepared via different plant resources, Ag NPs produced by *M. piperita* was the best, because it mostly consisted of tiny spherical densely distributed nanoparticles. While in Ag NPs prepared from *C. sativa*, the tiny nanoparticles had stuck together and formed bigger 'cauliflower'-like nanoclusters. In contrast, FESEM images of the samples prepared by *D. stramonium* and *P. orientale* displayed high agglomeration, and also the synthesized nanoparticles formed large aggregates with the size of 200 nm to 1.0 μm. Furthermore, the EDX patterns showed strong characteristic absorption signal of metallic silver nanocrystals around 3.1 keV (Figure 2-right). This intense Ag signal accompanied by some oxygen, carbon, and nitrogen peaks, which came from the plant biomolecules attaching to the Ag NPs [39]. The weak peaks of chlorine in the EDX patterns exhibited the presence of AgCl impurity in low levels, which had been already detected by XRD. Although, both XRD and EDX results approved that the purest Ag NPs was that produced using *M. piperita.* Considering all the above characterization results, *M. piperita* was accordingly selected as the best plant resource of choice to fabricate Ag NPs through solid-state route.

### 3.3. Optimization of biogenic Ag NPs synthesis using M. piperita through solid-state production

In the solid-state synthesis, the leaf powder/silver nitrate weight ratios and temperature are two main factors which could control the size and purity of the synthesized Ag NPs. At first, to investigate the effect of precursor's weight ratios in this study, the silver nitrate to *M. piperita* leaf powder ratios were changed as $m_{AgNO3}$: $m_{M.\ piperita\ powder}$ = 1:1, 1:2, and 1:3, at the same temperature of 600 °C. In the XRD patterns of the first two samples, the existence of intense signals at 38.1°, 44.2°, 64.6° and

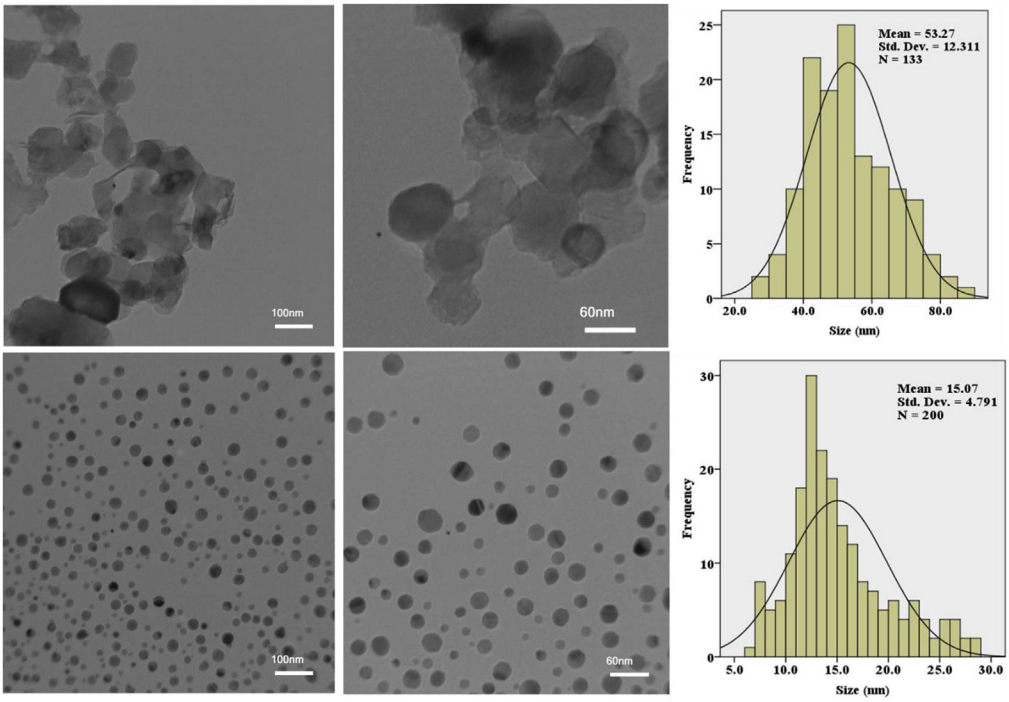


**Figure 5.** TEM images of Ag NPs in two different magnifications synthesized using *M. piperita* through solution-phase (top) and solid-state (bottom) method ($m_{AgNO3}$: $m_{M.\ piperita\ powder}$ = 1:2, and 600 °C), and their particle size distribution histograms.

77.4° approved the synthesis of crystalline Ag NPs (Figure 3a-c). In these patterns, the nonappearance of signals regarding to impurities confirmed the purity of synthesized Ag NPs. When the amount of *M. piperita* leaf powder was increased up to 1:3, slight impurity peaks were detectable in the XRD pattern (Figure 3a-c). It could be contributed to the fact that the increasing the plant powder masses, as a chloride source, might result in the production of little AgCl. Furthermore, FESEM analysis was employed to evaluate the size and morphology of the synthesized Ag NPs with different ratios of *M. piperita* (Figure 3d-f). It was observed that upon applying higher feeding ratios, uniform and separated spherical Ag NPs with no agglomeration could be formed. However, a reduction in the weight of *M. piperita* powder considerably led to the production of agglomerated nanoparticles with the larger size ranges. FESEM results revealed that *M. piperita* leaf powder could act as both capping and reducing agents in this process. On the other hand, according to the XRD results, the Ag NPs sample prepared using the leaf powder/silver nitrate weight ratios = 1:3 could be neglected due to the detection of slight impurity. Besides, based on the SEM images, Ag NPs sample synthesized by the leaf powder/silver nitrate weight ratios = 1:1 could be ignored, because in this ratio some agglomerated particles were prepared. Hence, considering the above-mentioned results, the vital role of the plant resource amounts in controlling the purity and the size of the final Ag NPs was approved. Therefore, the feeding ratio of ($m_{AgNO3}$: $m_{M.\ piperita\ powder}$ = 1:2) was selected as the optimum amount for the synthesis of Ag NPs, containing neither agglomerated particles nor impurities, using the solid-state route.

Figures 4a-c showed the XRD patterns of solid-state synthesized Ag NPs using *M. piperita* leaf powder at different temperatures. Four diffraction peaks of Ag NPs in the XRD patterns have confirmed the bio-reduction of silver nitrate and synthesis the crystalline Ag NPs. Besides these prominent Ag NPs signals, there were also weak peaks at $2\theta = 28.9°$ (012) and 32.5° (111) that could be indexed to the residual $AgNO_3$ and $Ag_2O$, respectively, which was remained in the samples because of incomplete decomposition of silver salt in temperatures below 500 °C [22, 23]. When the temperature of the calcination process was raised from 300 up to 600 °C, the impurity signals were decreased and entirely disappeared in the XRD pattern of Ag NPs produced at 600 °C. Afterwards, the dispersity and morphology of the Ag NPs prepared at different temperatures were investigated using SEM images (Figure 4d-f).

### 3.4. Proposed mechanism of biogenic Ag NPs synthesis using M. piperita through solid-state production

TEM microscopy was employed to better clarify the superiority of solid-state route over phase solution method as well as to explain the size and morphology of the as prepared Ag NPs. Figure 5 showed the TEM images of the samples prepared by *M. piperita* through solution and solid-state routes in two magnifications. TEM images of the solution-phase synthesized Ag NPs presented spherical nanoparticles with the particle size of 25–100 nm (average particle size of 53 nm). It seems that a layer of biomaterials has covered the as-prepared nanoparticles and sticks them to each other like glue. In contrast, it could be seen uniform and distinctly separated Ag NPs with the sizes ranging from 5 to 30 nm (average particle size of 15 nm) via solid-state method. It could be justified that the biomaterials which were responsible for reduction of $Ag^+$, were decomposed at high temperature through calcination process and so they did not attach to the surface of nanoparticles and their residuals were removed during washing.

*M. piperita* leaf main ingredients are phenolic acids (*i.e.*, rosmarinic and caffeic acids), flavones (*i.e.*, luteolin derivatives) and flavanones (*i.e.*, eriocitrin derivatives) which are reported as its principal antioxidant constituents and seem to be involved in the bio-reduction process of Ag ions to Ag NPs [40, 41]. Besides, essential oils (*i.e.*, oxygenated terpenes like menthol) in *M. piperita* together with polyphenols might be considered as the main contributors in the biogenic synthesis of Ag NPs [40]. Such biomaterials in the leaf composition of *M. piperita* leaf were not only responsible for the reduction of silver ions, but they also were able to stabilize synthesized nanoparticles as capping agents [41]. Considering these facts, probable mechanism for the formation of Ag NPs using caffeic acid, as one of the most prominent antioxidant constituents of the leaf powder of *M. piperita*, was depicted in Figure 6. It could be proposed that $Ag^+$ coordination to the hydroxyls of caffeic acids and formation of a

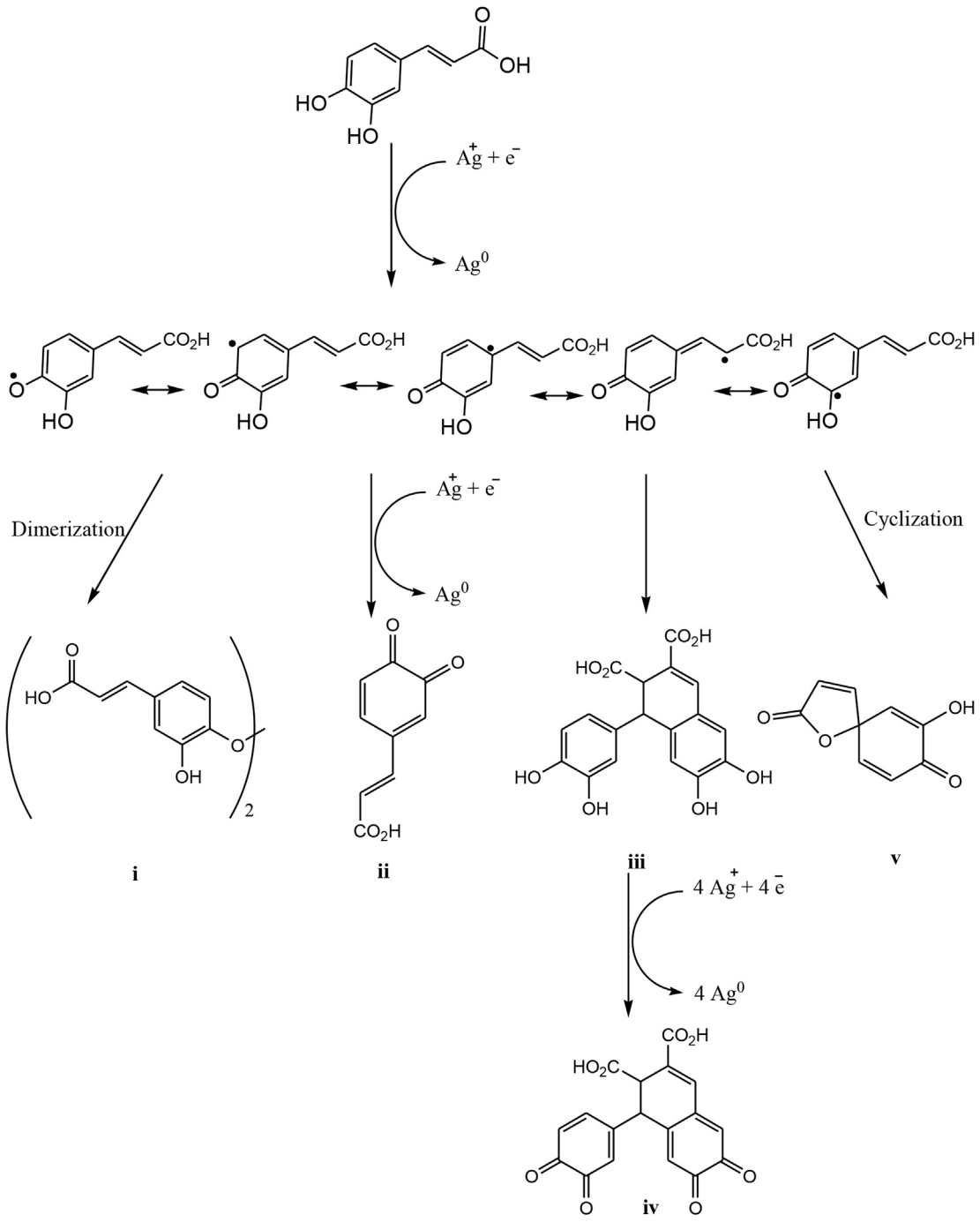


**Figure 6.** Possible mechanism of bio-reduction of silver nitrate to Ag NP using caffeic acid in *M. piperita*.

natural complex between them might result in electron transformation to Ag ions and production of well uniform and stabilized Ag NPs [42, 43]. Moreover, caffeic acid due to its structural characteristics could stabilize the formed phenoxy radicals, which explained its antioxidant character. Another hydroxyl group of the produced free radical could release a hydrogen ion and electron again to form a stable o-quinone compound (**ii**). Besides, oxidative dimerization of the first produced free radicals through a coupling reaction of semiquinone radicals resulted in the intermediate oxidative caffeic acid dimer (**iii**) whose four hydroxyl groups may also be oxidized to release four hydrogen ions and four electrons to form a quinone (**iv**) (Figure 6). Besides, high nucleophilicity of phenolic acids aromatic rings resulted in formation of chelate between their hydroxyl and carbonyl groups and silver ions [44]. Therefore, the large and bulky chemical structure of these phenolic acids, which surrounded the Ag ions, may result in the tiny Ag NPs production. After sintering at 600 °C, the organic materials were decomposed and this cause formation of Ag NPs which were small and distinctly separated from each other, as could be seen clearly in their TEM images.

### 3.5. Dye removal efficiency using as-prepared biogenic Ag NPs

After properly characterizing our samples, we performed the adsorption study to investigate the proficiency of the as-prepared Ag NPs in water treatment. The results displayed that CV removal efficiency

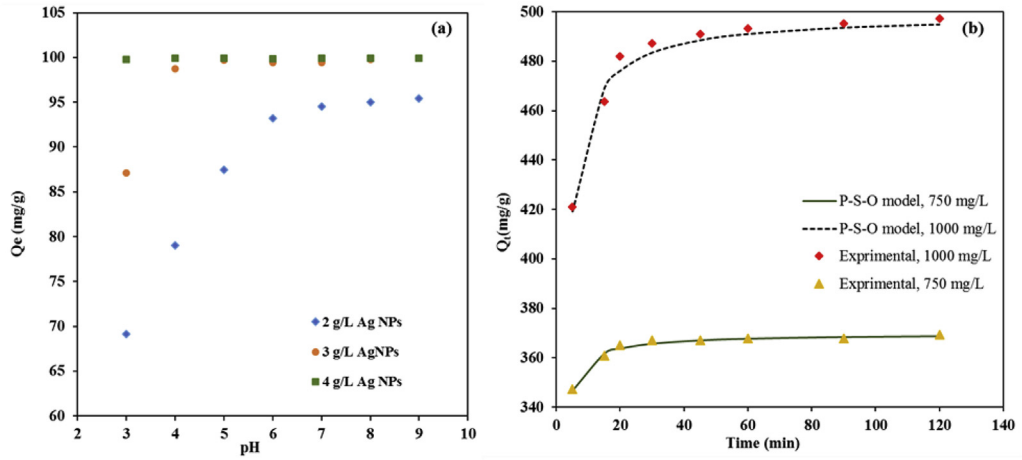


**Figure 7.** (a) Effects of initial solution pH on CV adsorption using different amounts of biogenic Ag NPs (temperature 25 °C, initial concentration of 1000 mg/L, shaking for 120 min). (b) Pseudo second order kinetic models of CV sorption using biogenic Ag NPs (2 g/L, pH = 9, with two initial concentrations of 750 and 1000 mg/L).

remarkably increased upon enhancing the Ag NPs dosages, which might be rationalized by the larger accessible specific areas and more unsaturated sites for sorption. Typically, for removal of CV from water, dosage of the adsorbents was varied in the range of 0.2–6 g/L in the literature [30, 32, 45, 46, 47, 48], hence in this study we examined three different Ag NPs amounts (i.e., 2, 3 and 4 g/L) for adsorption e. For instance, at pH of 3, when the dosage of Ag NPs was doubled from 2 g/L to 4 g/L, the CV removal ability was increased from 69.1 to 99.8% – an increment of 30% (Figure 7a). More specifically, the key role of pH parameter was more perceptible in the lower amounts of nanoadsorbent (i.e., at Ag NPs dosage of 2 g/L). Under such conditions, increasing the pH of CV solutions from 3.0 to 9.0 could lead to raising the percentage of CV removal from 69.1 to 95.4 mg/g (Figure 7a). Since CV is considered as a cationic dye, it could be favorably adsorbed on negatively charged surfaces. With increasing of pH, the surface negative charge of the nanoparticles increased which resulting in an enhancement of the electrostatic attractions between the adsorbent and CV molecules and consequently improving the CV removal percentage [49]. The CV removal efficiency was found to be more pH-dependent at lower dosages of nanoadsorbent (limited active sorption sites), while for higher dosages of nanoadsorbent nearly the same removal (%) efficiencies were observed in the entire pH range. On the other word, at pH = 9, the CV elimination occurred profoundly in high level even at low Ag NPs dosage.

For example, when the Ag NPs dosage was adjusted at 2 g/L, the CV removal (%) efficiencies were estimated as 93.2%, 94.5%, and 95.7% at pH of 6, 7, and 9, respectively. Moreover, the optimum pH of 9 for removal of CV from water have been reported in several earlier works [30, 49, 50]. As a result, for preparing optimum conditions, pH value of 9 and adsorbent dosage of 2 g/L were chosen for CV removal, and utilized then in further experiments.

To study the kinetics of sorption process, the removal of CV versus contact time was assessed at two initial CV concentrations (750 and 1000 mg/L) (Figure 7b). The pseudo-first-order (P–F–O) and pseudo-second-order (P–S–O) kinetic models were employed, whose liner equations were the following equations of (6) and (7), respectively [36, 51, 52]:

$$dq_t / dt = k_1(q_e - q_t) \quad (6)$$

$$dq_t / dt = k_2(q_e - q_t)^2 \quad (7)$$

where the contact time is expressed as $t$ (min); the rate constants are named as $k_1$ ($min^{-1}$) and $k_2$ (g $mg^{-1}$ $min^{-1}$), and the $q_t$ and $q_e$ (mg $g^{-1}$) correspond to the CV amounts which adsorbed at time t and equilibrium, respectively.

The P–S–O equation fitted well with the experimental data, and the adjusted regression coefficients ($R^2_{adj}$) were 0.9870 and 0.9969 for initial CV concentrations of 750 and 1000 mg/L, respectively (Figure 7b and Table 2). It was also observed that the amounts of $k_2$ parameter were decreased from 0.0081 to 0.0021 g $mg^{-1}$ $min^{-1}$ with the enhancement of CV initial concentration from 750 to 1000 mg/L, respectively. This could be attributed to the increase in CV uptake upon rising the initial concentration of dye [49].

Moreover, based on the P–S–O model, for determination of the required time for half and 95% of saturation ($q_e$), $t_{1/2}$ and $t_{0.95}$ parameters were estimated, respectively (Table 2) [36, 37]. For both initial CV concentrations, about half of the CV molecules were removed through sorption during the first minute of the experiment (Table 2). This would be attributed to the load of active sites for sorption on the Ag NPs surface at the beginning of the sorption experiment. This followed by a slower adsorption, which lastly reached an equilibrium due to the sorption site saturation/deactivation on the nanoadsorbent surface. Finally, the adsorption was terminated during 20 min ($t_{0.95}$, Table 2) and after that there were no significant changes in adsorption efficiency (Figure 7b, Table 2).

Furthermore, to investigate the adsorption capacity of Ag NPs, the isotherm data were analyzed based on the Langmuir and Freundlich models using the following equations of (8(8) and (9)(9), respectively [36].

$$q_e = \frac{(q_m K_L C_e)}{1 + K_L C_e} \quad (8)$$

**Table 2.** Parameters of P–S–O and P–F–O kinetic models for the adsorption of CV onto biogenic Ag NPs.

| P–S–O | | | | | | P–F–O | | | |
|---|---|---|---|---|---|---|---|---|---|
| Initial concentration (mg/L) | $q_e$ (mg/g) | $k_2$ (g $mg^{-1}$ $min^{-1}$) | $R^2_{adj}$ | $t_{1/2}$ (min) | $t_{0.95}$ (min) | SD (mg/g) | $k_1$ ($min^{-1}$) | $R^2_{adj}$ | SD (mg/g) |
| 750 | 370.4 | 0.0081 | 0.9638 | 0.33 | 5.75 | 0.96 | 0.0012 | 0.729 | 13.51 |
| 1000 | 500.0 | 0.0021 | 0.9801 | 0.95 | 18.07 | 3.74 | 0.0502 | 0.8525 | 5.42 |

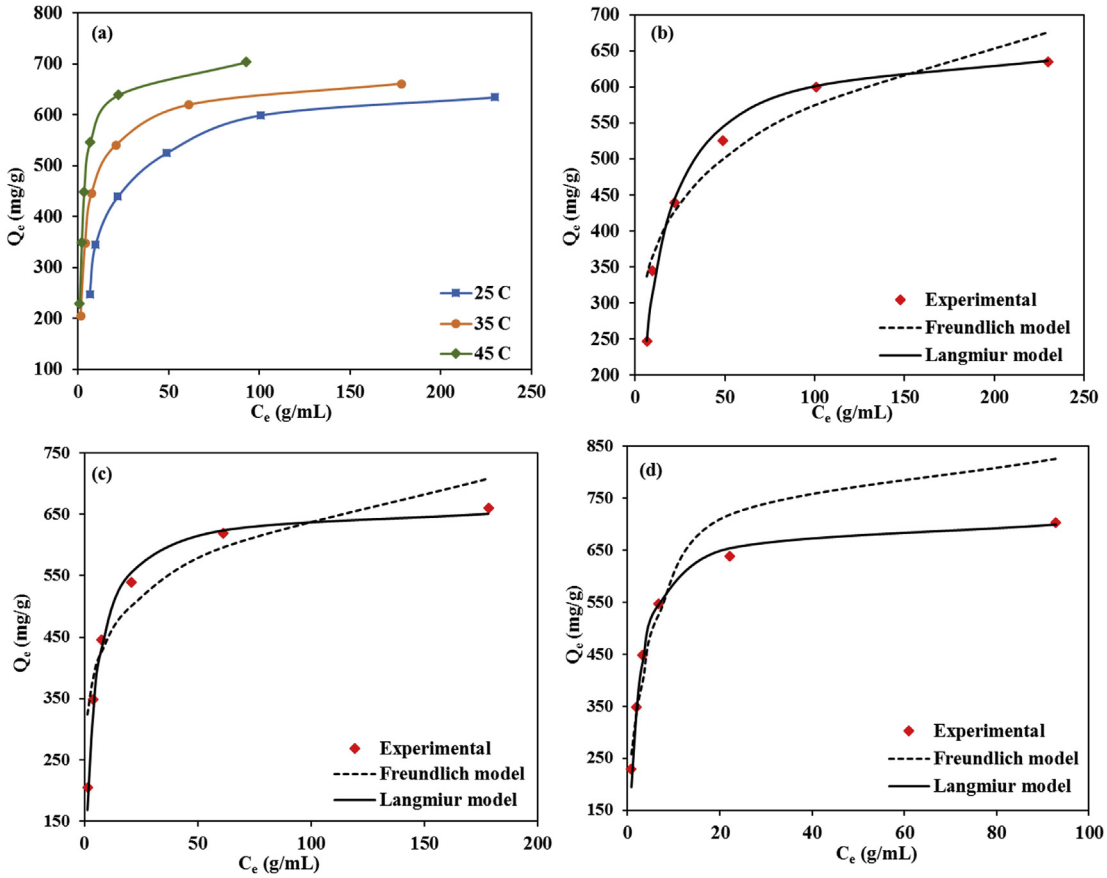


**Figure 8.** (a) Sorption isotherms of CV on the biogenic Ag NPs at three different temperatures (2 g/L, pH = 9), and the non-linear fitting of Langmuir and Freundlich isotherm models at temperature of (b) 25 °C (c) 35 °C and (d) 45 °C.

**Table 3.** Isotherm constants for the sorption isotherm models of CV onto biogenic Ag NPs.

| Temperature (K) | Langmuir | | | | Freundlich | | | |
|---|---|---|---|---|---|---|---|---|
| | $q_m$ (mg/g) | $K_L$ (L/mg) | $R^2_{adj}$ | *SD* mg·g$^{-1}$ | $K_F$ mg·g$^{-1}$·(mg·L$^{-1}$)$^{-1/n}$ | n | $R^2_{adj}$ | *SD* mg·g$^{-1}$ |
| 293 | 666.7 | 0.0909 | 0.9883 | 17.88 | 234.07 | 5.128 | 0.8723 | 48.12 |
| 303 | 671.1 | 0.2403 | 0.9777 | 23.05 | 306.95 | 6.199 | 0.8317 | 63.40 |
| 313 | 704.7 | 0.4827 | 0.9841 | 16.97 | 277.63 | 3.262 | 0.8660 | 61.07 |

**Table 4.** Thermodynamic parameters for the adsorption of CV onto biogenic Ag NPs.

| Temperature (K) | $K_L$ (L/mol) | $\Delta G^0$ (kJ/mol) | $\Delta S^0$ (J/mol·K) | $\Delta H^0$ (kJ/mol) |
|---|---|---|---|---|
| 298 | 37088.2 | -26.06 | 308.8 | 65.87 |
| 308 | 98044.4 | -29.43 | | |
| 318 | 196951.0 | -32.23 | | |

pH = 9.0; nanoadsorbent amount: 2 g/L; contact time: 120 min.

$$q_e = K_F \times C_e^{\frac{1}{n_F}} \quad (9)$$

In the Langmuir model, the adsorbed amount of dye and the CV concentration at equilibrium are expressed as $q_e$ (mg/g) and $C_e$ (mg/L), respectively; the $K_L$ (L/mg) corresponds to sorption energy, and $q_m$ (mg/g) is the maximum adsorption capacity. In the Freundlich model, $K_F$ and $n$ are the Freundlich constant and an empirical denoting the sorption intensity, respectively.

Based on the isotherm study results the dye sorption process was found to be temperature dependent, and the CV removal was considerably increased with increasing temperature, indicating the adsorption process was endothermic (Figure 8a). Table 3 showed the calculated adjusted regression coefficients ($R^2_{adj}$) and standard deviation of residues (SD). These data exposed the better fitting of Langmuir than the Freundlich model with the sorption experiment (Figure 8b-c). Hence, based on the Langmuir isotherm, the CV sorption capacity of biogenic nanoadsorbent was found to be 704.7 mg/g which was consistent with the experimental results (698.7 mg/g), at 45 °C and initial dye concentration of 1500 mg/L, and proposed a reversible physisorption mechanism.

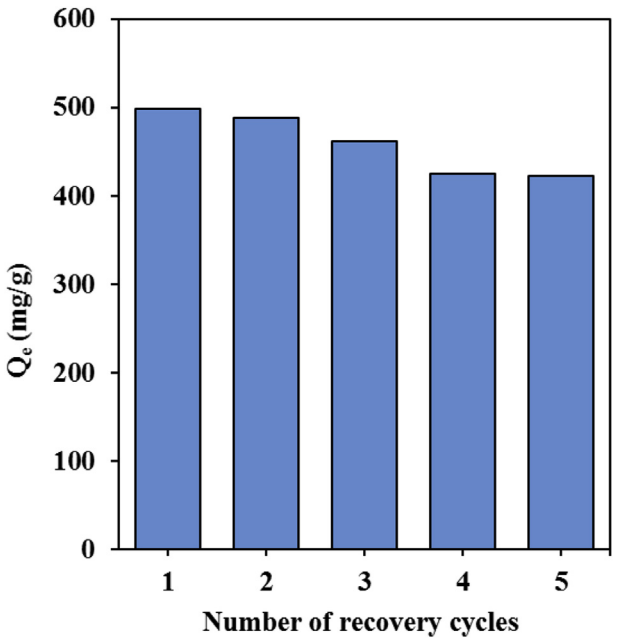


**Figure 9.** Comparison of adsorption efficiency of biogenic Ag NPs over several consecutive recovery cycles.

Consequently, to explain the feasibility of sorption process, the thermodynamic data, including change in enthalpy ($\Delta H^0$), Gibbs free energy ($\Delta G^0$), and entropy ($\Delta S^0$) were investigated. The following equations Eq. (10) - Eq. (12) were used for calculation of such parameters [37, 49]:

$$\Delta G^0 = \Delta H^0 - T\Delta S \tag{10}$$

$$\Delta G^0 = -\mathrm{RT}\ln \mathrm{K} \tag{11}$$

$$ln(K_c) = \frac{\Delta S^0}{R} - \frac{\Delta H^0}{RT} \tag{12}$$

where $R = 8.314$ J/mol·K (ideal gas constant), temperature is expressed as $T$ (K) and Langmuir constant (L/mol) is named as $K$ in the equation. The $\Delta S^0$ (J/mol·K) and $\Delta H^0$ (kJ/mol) were calculated from the intercepts and slopes of the ln $K$ against $1/T$ curves (Table 4).

Based on the above results, the estimated $\Delta G^0$ was found to be between -26.0 to -32.2 kJ/mol, so it was possibly deduced that the sorption was a physical spontaneous process [49, 53, 54]. The decrement of $\Delta G^0$ with the rising of the temperature corresponded to a reduction in spontaneity degree at higher temperatures [53, 54]. The $\Delta H^0$ value was positive (65.87 kJ/mol) which approved the endothermic sorption process, which mostly induced by physical interactions including, H-bonding forces and exchange of dentate [53, 54]. Moreover, the positive value of $\Delta S^0$ (308.8 J/mol·K) represented that the adsorption of CV would result in desorption of the solvent [53, 54].

On the other word, although the adsorption of CV decreased the entropy of the sorption by diminishing the freedom, desorption of water caused an enhancement in the entropy. The adsorption of each CV molecule led to desorption of several water molecules and subsequently the entropy changes were positive.

To evaluate the reusability of biogenic Ag NPs, nanoadsorbents were collected, recovered, and reused after its fresh adsorption run. The results displayed that after the first recovery cycle, Ag NPs could maintain its capacity the same as its fresh form (498.2 mg/g). Through the next reuse runs, the sorption capacity of the Ag NPs stayed still in high values (i.e., 422.5 mg/g after 5$^{th}$ cycle), which corresponded 15% decrement in adsorption capacity after five reusing steps (Figure 9a). Such typical reduction in sorption efficiency of adsorbents after several reusing runs might be resulted from not perfect regeneration process. In fact, after each cycle, a few amounts of the adsorbed CV molecules may remain on the nanoadsorbent and then inactive its accessible sites.

To provide more information about the significance of the as-synthesized biogenic Ag NPs, the efficiency of the current nanoadsorbent in CV removal was compared to the other previously reported nanoadsorbents (Table 5). The adsorption capacity ($q_m$) of Ag NPs nanoadsorbent was greater than other adsorbents which approved its high performance in the removal of dye from water. Moreover, comparison between the performance of biogenic Ag NPs produced through solid-state synthesis using *M. piperita* with the other reported green-synthesized silver nanoparticles approved the superiority of the present Ag NPs [55]. For example, Ag nanoparticles reduced by *Kyllinga brevifolia* have been utilized for removal of methylene blue [56], Ag NPs synthesized using *Solanum nigrum* and *Cannabis sativa* were employed for removal of some textile dyes [57], starched-Ag NPs prepared by aqueous extracts of *Malus domestica-Green* Delicious and *Lagenaria siceraria* were studied for malachite Green [58], biosynthesized Ag NPs from cobweb have been used for removal of rhodamine B [59]. The higher sorption capacity of the present Ag NPs compared to the as-mentioned studies may be due to the combination of the solid-state synthetic method and *M. piperita* leaf powder, which could finally result in the production of small, uniform, and pure Ag NPs with high surface-active sites. Meanwhile, according to the characterization results of nanoparticles, in bio-reduction of $Ag^+$ ions via *M. piperita*, the plant leaf powder played two critical roles: i) as a reducing agent; and ii) as a protector to stabilize Ag NPs. Altogether, simple adjustment of the precursor's ratio and the temperature could provide small, stable and pure Ag NPs with narrow size distribution and high active surface area with proficient sorption performance in removal of crystal violet from water.

## 4. Conclusions

Small spherical and entirely pure Ag NPs with high crystalline structure, uniform size distribution, and without any aggregation could be obtained using the solid-state biosynthesis approach. *M. piperita* leaf powder might serve as an appropriate reducing/stabilizing plant mediator towards biogenic Ag NPs in large-scale production. Moreover, adjusting the weight ratio of *M. piperita* leaf powder/$AgNO_3$ as well as the temperature of the reaction were distinguished as two effective

**Table 5.** Comparison with other adsorbents.

| Adsorbent | Dye | Optimum pH | $q_m$ (mg/g) | Ref. |
|---|---|---|---|---|
| Silver nanoparticles immobilized on the activated carbon | CV | 7 | 87.2 | [32] |
| Soil-silver nanocomposite | CV | 4.7 | 1.9 | [60] |
| Functionalised multi-walled carbon nanotubes | CV | 8 | 90.5 | [61] |
| Surfactant modified magnetic nanoadsorbent | CV | 6 | 166.7 | [53] |
| Magnetically modified activated carbon | CV | 9 | 67.1 | [62] |
| Biogenic $\beta$-CD functionalized $Fe^{\circ}$ NPs | CV | 9 | 454.5 | [30] |
| ***M. piperita* derived Ag NPs *via* solid-state synthesis** | **CV** | **9** | **704.7** | **this work** |

parameters, which could control and manage the size, dispersity, and purity of as-prepared biogenic Ag NPs. Lastly, the current green synthesized Ag NPs could be considered as a superior, eco-friendly and cost-effective nanoadsorbent for water remediation purposes.

## Declarations

### *Author contribution statement*

Mohsen Rahimi Sharbaf Moghadas: Conceived and designed the experiments; Performed the experiments.

Elaheh Motamedi: Conceived and designed the experiments; Analyzed and interpreted the data; Contributed reagents, materials, analysis tools or data; Wrote the paper.

Jaber Nasiri: Performed the experiments; Wrote the paper.

Mohammad Reza Naghavi, Manije Sabokdast: Contributed reagents, materials, analysis tools or data; Wrote the paper.

### *Funding statement*

This research did not receive any specific grant from funding agencies in the public, commercial, or not-for-profit sectors.

### *Competing interest statement*

The authors declare no conflict of interest.

### *Additional information*

No additional information is available for this paper.

## References

[1] S. Lin, W. Zhu, Y. Jin, K.B. Crozier, Surface enhanced Raman scattering with Ag nanoparticles optically trapped by a photonic crystal cavity, Nano Lett. 13 (2013) 559–563.

[2] B.M. Abu-Zied, A.M. Asiri, An investigation of the thermal decomposition of silver acetate as a precursor for nano-sized Ag-catalyst, Thermochim. Acta 581 (2014) 110–117.

[3] V. Dhand, L. Soumya, S. Bharadwaj, S. Chakra, D. Bhatt, B. Sreedhar, Green synthesis of silver nanoparticles using Coffea arabica seed extract and its antibacterial activity, Mater. Sci. Eng. C 58 (2016) 36–43.

[4] J. Peng, J. Lin, Z. Chen, M. Wei, Y. Fu, S. Lu, D. Yu, W. Zhao, Enhanced antimicrobial activities of silver-nanoparticle-decorated reduced graphene nanocomposites against oral pathogens, Mater. Sci. Eng. C 71 (2017) 10–16.

[5] Y. Zhou, K. Hu, Z. Guo, K. Fang, X. Wang, F. Yang, N. Gu, PLLA microcapsules combined with silver nanoparticles and chlorhexidine acetate showing improved antibacterial effect, Mater. Sci. Eng. C 78 (2017) 349–353.

[6] L.K. Ruddaraju, P.N.V.K. Pallela, S.V.N. Pammi, V.S. Padavala, V.R.M. Kolapalli, Synergetic antibacterial and anticarcinogenic effects of Annona squamosa leaf extract mediated silver nano particles, Mater. Sci. Semicond. Process. 100 (2019) 301–309.

[7] P.N.V.K. Pallela, S. Ummey, L.K. Ruddaraju, S.V.N. Pammi, S.G. Yoon, Ultra Small, mono dispersed green synthesized silver nanoparticles using aqueous extract of Sida cordifolia plant and investigation of antibacterial activity, Microb. Pathog. 124 (2018) 63–69.

[8] S. Kantipudi, L. Pethakamsetty, S.M. Kollana, J.R. Sunkara, P. Kollu, N.R. Parine, M. Rallabhandi, S.V. Narayana Pammi, Diospyros assimilis root extract assisted biosynthesised silver nanoparticles and their evaluation of antimicrobial activity, IET Nanobiotechnol. 12 (2018) 133–137.

[9] R. Lakshmi Kalyani, V.S. Chandra, P.P.N. Vijaykumar, S.V.N. Pammi, M. Rajkumar, P.V. Swamy, K.V.R. Murthy, Biosynthesis of silver nanoparticles using annona squamosa leaf extract with synergistic antibacterial activity, Indian J. Pharmaceut. Sci. 81 (2019) 1036–1044.

[10] L. Pethakamsetty, K. Kothapenta, H.R. Nammi, L.K. Ruddaraju, P. Kollu, S.G. Yoon, S.V.N. Pammi, Green synthesis, characterization and antimicrobial activity of silver nanoparticles using methanolic root extracts of Diospyros sylvatica, J. Environ. Sci. (China) 55 (2017) 157–163.

[11] P.P.N. Vijay Kumar, R.L. Kalyani, S.C. Veerla, P. Kollu, U. Shameem, S.V.N. Pammi, Biogenic synthesis of stable silver nanoparticles via Asparagus racemosus root extract and their antibacterial efficacy towards human and fish bacterial pathogens, Mater. Res. Express 6 (2019) 104008.

[12] V. Ahluwalia, J. Kumar, R. Sisodia, N.A. Shakil, S. Walia, Green synthesis of silver nanoparticles by Trichoderma harzianum and their bio-efficacy evaluation against Staphylococcus aureus and Klebsiella pneumonia, Ind. Crop. Prod. 55 (2014) 202–206.

[13] A.K. Mittal, Y. Chisti, U.C. Banerjee, Synthesis of metallic nanoparticles using plant extracts, Biotechnol. Adv. 31 (2013) 346–356.

[14] R. Sithara, P. Selvakumar, C. Arun, S. Anandan, P. Sivashanmugam, Economical synthesis of silver nanoparticles using leaf extract of Acalypha hispida and its application in the detection of Mn ( II ) ions, J. Adv. Res. 8 (2017) 561–568.

[15] I. Fatimah, Green synthesis of silver nanoparticles using extract of Parkia speciosa Hassk pods assisted by microwave irradiation, J. Adv. Res. 7 (2016) 961–969.

[16] S. Ahmed, M. Ahmad, B.L. Swami, S. Ikram, A review on plants extract mediated synthesis of silver nanoparticles for antimicrobial applications: a green expertise, J. Adv. Res. 7 (2016) 17–28.

[17] L. Wang, Y. Wu, J. Xie, S. Wu, Z. Wu, Characterization , antioxidant and antimicrobial activities of green synthesized silver nanoparticles from Psidium guajava L . leaf aqueous extracts, Mater. Sci. Eng. C 86 (2018) 1–8.

[18] S. Park, S. Cha, I. Cho, S. Park, Y. Park, S. Cho, Y. Park, Antibacterial nanocarriers of resveratrol with gold and silver nanoparticles, Mater. Sci. Eng. C 58 (2016) 1160–1169.

[19] D. Debnath, C. Kim, S.H. Kim, K.E. Geckeler, Solid-state synthesis of silver nanoparticles at room temperature: poly(vinylpyrrolidone) as a tool, Macromol. Rapid Commun. 31 (2010) 549–553.

[20] M. Goudarzi, N. Mir, M. Mousavi-Kamazani, S. Bagheri, M. Salavati-Niasari, Biosynthesis and characterization of silver nanoparticles prepared from two novel natural precursors by facile thermal decomposition methods, Sci. Rep. 6 (2016) 32539.

[21] A.M. Abdelgawad, M.E. El-Naggar, W.H. Eisa, O.J. Rojas, Clean and high-throughput production of silver nanoparticles mediated by soy protein via solid state synthesis, J. Clean. Prod. 144 (2017) 501–510.

[22] K. Otto, I. Oja Acik, M. Krunks, K. Tõnsuaadu, A. Mere, Thermal decomposition study of HAuCl4·3H2O and AgNO3 as precursors for plasmonic metal nanoparticles, J. Therm. Anal. Calorim. 118 (2014) 1065–1072.

[23] S.M. Hosseinpour-Mashkani, M. Ramezani, Silver and silver oxide nanoparticles: synthesis and characterization by thermal decomposition, Mater. Lett. 130 (2014) 259–262.

[24] J. Kwiczak-Yiğitbaşi, Ö. Laçin, M. Demir, R.E. Ahan, U.Ö.Ş. Şeker, B. Baytekin, A sustainable preparation of catalytically active and antibacterial cellulose metal nanocomposites: via ball milling of cellulose, Green Chem. 22 (2020) 455–464.

[25] M. Baláž, N. Daneu, Ľ. Balážová, E. Dutková, Ľ. Tkáčiková, J. Briančin, M. Vargová, M. Balážová, A. Zorkovská, P. Baláž, Bio-mechanochemical synthesis of silver nanoparticles with antibacterial activity, Adv. Powder Technol. 28 (2017) 3307–3312.

[26] R.A.D. Arancon, A.M. Balu, A.A. Romero, M. Ojeda, M. Gomez, J. Blanco, J.L. Domingo, R. Luque, Mechanochemically synthesized Ag-based nanohybrids with unprecedented low toxicity in biomedical applications, Environ. Res. 154 (2017) 204–211.

[27] M.J. Rak, T. Friščić, A. Moores, One-step, solvent-free mechanosynthesis of silver nanoparticle-infused lignin composites for use as highly active multidrug resistant antibacterial filters, RSC Adv. 6 (2016) 58365–58370.

[28] J. Nasiri, M. Rahimi, Z. Hamezadeh, E. Motamedi, M.R. Naghavi, Fulfillment of green chemistry for synthesis of silver nanoparticles using root and leaf extracts of Ferula persica: solid-state route vs. solution-phase method, J. Clean. Prod. 192 (2018) 514–530.

[29] M.K. Satapathy, P. Das, Optimization of crystal violet dye removal using novel soil-silver nanocomposite as nanoadsorbent using response surface methodology, J. Environ. Chem. Eng. 2 (2014) 708–714.

[30] J. Nasiri, E. Motamedi, M.R. Naghavi, M. Ghafoori, Removal of crystal violet from water using β-cyclodextrin functionalized biogenic zero-valent iron nanoadsorbents synthesized via aqueous root extracts of Ferula persica, J. Hazard Mater. 367 (2019) 325–338.

[31] K. Dastafkan, M. Khajeh, M. Bohlooli, M. Ghaffari-Moghaddam, N. Sheibani, Mechanism and behavior of silver nanoparticles in aqueous medium as adsorbent, Talanta 144 (2015) 1377–1386.

[32] A.H. AbdEl-Salam, H.A. Ewais, A.S. Basaleh, Silver nanoparticles immobilised on the activated carbon as efficient adsorbent for removal of crystal violet dye from aqueous solutions. A kinetic study, J. Mol. Liq. 248 (2017) 833–841.

[33] K. Vijayaraghavan, S.P.K. Nalini, N.U. Prakash, D. Madhankumar, One step green synthesis of silver nano/microparticles using extracts of Trachyspermum ammi and Papaver somniferum, Colloids Surf. B Biointerfaces 94 (2012) 114–117.

[34] D. MubarakAli, N. Thajuddin, K. Jeganathan, M. Gunasekaran, Plant extract mediated synthesis of silver and gold nanoparticles and its antibacterial activity against clinically isolated pathogens, Colloids Surf. B Biointerfaces 85 (2011) 360–365.

[35] M. Gomathi, P.V. Rajkumar, A. Prakasam, K. Ravichandran, Green synthesis of silver nanoparticles using Datura stramonium leaf extract and assessment of their antibacterial activity, Resour. Technol. 3 (2017) 280–284.

[36] P.S. Thue, A.C. Sophia, E.C. Lima, A.G.N. Wamba, W.S. de Alencar, G.S. dos Reis, F.S. Rodembusch, S.L.P. Dias, Synthesis and characterization of a novel organic-inorganic hybrid clay adsorbent for the removal of acid red 1 and acid green 25 from aqueous solutions, J. Clean. Prod. 171 (2018) 30–44.

[37] A.J.B. Leite, E.C. Lima, G.S. Dos Reis, P.S. Thue, C. Saucier, F.S. Rodembusch, S.L.P. Dias, C.S. Umpierres, G.L. Dotto, Hybrid adsorbents of tannin and APTES (3-aminopropyltriethoxysilane) and their application for the highly efficient removal of acid red 1 dye from aqueous solutions, J. Environ. Chem. Eng. 5 (2017) 4307–4318.

[38] K. Murugan, D. Dinesh, P.J. Kumar, C. Panneerselvam, J. Subramaniam, P. Madhiyazhagan, U. Suresh, M. Nicoletti, A.A. Alarfaj, M.A. Munusamy, A. Higuchi, H. Mehlhorn, G. Benelli, Datura metel-synthesized silver nanoparticles

magnify predation of dragonfly nymphs against the malaria vector Anopheles stephensi, Parasitol. Res. 114 (2015) 4645–4654.
[39] T.Y. Suman, D. Elumalai, P.K. Kaleena, R.S.R. Rajasree, GC-MS analysis of bioactive components and synthesis of silver nanoparticle using Ammannia baccifera aerial extract and its larvicidal activity against malaria and filariasis vectors, Ind. Crop. Prod. 47 (2013) 239–245.
[40] L.G. Riachi, C.A.B. De Maria, Peppermint antioxidants revisited, Food Chem. 176 (2015) 72–81.
[41] A. Sarkar, S.P. Shukla, S. Adhikari, T. Mukherjee, Synthesis , stabilisation and surface modification of gold and silver nanoparticles by rosmarinic acid and its analogues Anjana Sarkar , Shashi P . Shukla, Int. J. Nanotechnol. 7 (2010) 1027–1037.
[42] G. Vijayalakshmi, M. Adinarayana, P.J. Rao, Kinetics and mechanisms of oxidation of some antioxidants with photochemically generated tert-butoxyl radicals, Indian J. Biochem. Biophys. 47 (2010) 292–297.
[43] Y.S. Liu, Y.C. Chang, H.H. Chen, Silver nanoparticle biosynthesis by using phenolic acids in rice husk extract as reducing agents and dispersants, J. Food Drug Anal. 26 (2018) 649–656.
[44] V.K. Vidhu, S.A. Aromal, D. Philip, Green synthesis of silver nanoparticles using Macrotyloma uniflorum, Spectrochim. Acta Part A Mol. Biomol. Spectrosc. 83 (2011) 392–397.
[45] I. Ali, C. Peng, Z.M. Khan, M. Sultan, Green synthesis of phytogenic magnetic nanoparticles and their applications in the adsorptive removal of crystal violet from aqueous solution, Arabian J. Sci. Eng. 43 (2018) 6245–6246.
[46] A. Saeed, M. Sharif, M. Iqbal, Application potential of grapefruit peel as dye sorbent: kinetics, equilibrium and mechanism of crystal violet adsorption, J. Hazard Mater. 179 (2010) 564–572.
[47] J. Qin, F. Qiu, X. Rong, J. Yan, H. Zhao, D. Yang, Adsorption behavior of crystal violet from aqueous solutions with chitosan-graphite oxide modified polyurethane as an adsorbent, J. Appl. Polym. Sci. 132 (2015) 1–10.
[48] A. Pourjavadi, S.H. Hosseini, F. Seidi, R. Soleyman, Magnetic removal of crystal violet from aqueous solutions using polysaccharide-based magnetic nanocomposite hydrogels, Polym. Int. 62 (2013) 1038–1044.
[49] Y. Zhou, M. Zhang, X. Wang, Q. Huang, Y. Min, T. Ma, J. Niu, Removal of crystal violet by a novel cellulose-based adsorbent: comparison with native cellulose, Ind. Eng. Chem. Res. 53 (2014) 5498–5506.
[50] J.D. Fisk, R. Batten, G. Jones, J.P. O'Reilly, A.M. Shaw, pH Dependence of the crystal violet adsorption isotherm at the silica-water interface, J. Phys. Chem. B 109 (2005) 14475–14480.
[51] İ. Günay, E.B. Orman, A. Altındal, B. Salih, M. Özer, A.R. Özkaya, Novel tetrakis 4-(hydroxymethyl)-2,6-dimethoxyphenoxyl substituted metallophthalocyanines: synthesis, electrochemical redox, electrocatalytic oxygen reducing, and volatile organic compounds sensing and adsorption properties, Dyes Pigments 154 (2018) 172–187.
[52] A.A.A. Darwish, M. Rashad, H.A. Al-aoh, Methyl orange adsorption comparison on nanoparticles: isotherm, kinetics, and thermodynamic studies, Dyes Pigments 160 (2018) 563–571.
[53] C. Muthukumaran, V.M. Sivakumar, M. Thirumarimurugan, Adsorption isotherms and kinetic studies of crystal violet dye removal from aqueous solution using surfactant modified magnetic nanoadsorbent, J. Taiwan Inst. Chem. Eng. 63 (2016) 354–362.
[54] A.A. Jalil, S. Triwahyono, M.R. Yaakob, Z.Z.A. Azmi, N. Sapawe, N.H.N. Kamarudin, H.D. Setiabudi, N.F. Jaafar, S.M. Sidik, S.H. Adam, B.H. Hameed, Utilization of bivalve shell-treated Zea mays L. (maize) husk leaf as a low-cost biosorbent for enhanced adsorption of malachite green, Bioresour. Technol. 120 (2012) 218–224.
[55] Y. Zhang, B. Wu, H. Xu, H. Liu, M. Wang, Y. He, B. Pan, Nanomaterials-enabled water and wastewater treatment, NanoImpact 3–4 (2016) 22–39.
[56] N. Isa, Z. Lockman, Methylene blue dye removal on silver nanoparticles reduced by Kyllinga brevifolia, Environ. Sci. Pollut. Res. 26 (2019) 11482–11495.
[57] K. N, S. M, Efficient removal of toxic textile dyes using silver nanocomposites, J. Nanosci. Curr. Res. 2 (2017) 113–118.
[58] S. Muzaffar, H. Tahir, Enhanced synthesis of silver nanoparticles by combination of plants extract and starch for the removal of cationic dye from simulated waste water using response surface methodology, J. Mol. Liq. 252 (2018) 368–382.
[59] L. Azeez, A. Lateef, S.A. Adebisi, A.O. Oyedeji, Novel biosynthesized silver nanoparticles from cobweb as adsorbent for Rhodamine B: equilibrium isotherm, kinetic and thermodynamic studies, Appl. Water Sci. 8 (2018) 1–12.
[60] M.K. Satapathy, P. Das, Assessment on the modelling of the kinetic parameter for the removal of crystal violet dye using Ag-soil nanocomposite: linear and non-linear analysis, Desalin. Water Treat. 57 (2016) 4073–4080.
[61] V. Sabna, S.G. Thampi, S. Chandrakaran, Adsorption of crystal violet onto functionalised multi-walled carbon nanotubes: equilibrium and kinetic studies, Ecotoxicol. Environ. Saf. 134 (2016) 390–397.
[62] S. Hamidzadeh, M. Torabbeigi, S.J. Shahtaheri, Removal of crystal violet from water by magnetically modified activated carbon and nanomagnetic iron oxide, J. Environ. Heal. Sci. Eng. 13 (2015) 8.